で広がることが予想される。そのためにもより廉価な診断法の開発が必要であろう。

●謝辞

著者らの研究には科学技術振興調整費，独立行政法人医薬基盤研究所の「保健医療分野における基礎研究推進事業」，厚生労働科学研究費補助金の「基礎研究成果の臨床応用推進研究事業」，同「長寿科学総合研究事業」，新エネルギー・産業技術総合開発機構(NEDO)産業技術研究助成事業の支援をいただきました。またBF研究所に出資していただきました医薬品医療機器総合機構および各社に感謝いたします。本研究には「平成16年度三井住友海上福祉財団研究助成金」，「ノバルティス老化および老年医学研究基金」，「アストラゼネカ・リサーチグラント」の支援をいただきました。最後に共同研究者の福祉村病院　長寿医学研究所　赤津裕康，山本孝之，東北大学医学部　老年／漢方内科　荒井啓行，同機能薬理学分野 谷内 一彦　諸先生，旧BF研究所アミロイドイメージング研究チームおよび現東北大学PETイメージング研究チームの同僚に感謝の意を表します。

【参考・引用文献】

1) D. Schenk et al. : *Nature*, **400**, 173-177(1999).
2) H. Hara et al. : *Alzheimer's & Dementia*, **2**(3)Suppl 2, S611(2006).
3) T. Kimura et al. : *Bioorg. Med. Chem. Lett.*, **14**, 1527-1531(2004).
4) T. Kimura et al. : *Bioorg. Med. Chem. Lett.*, **15**, 211-215(2005).
5) I. Peretto et al. : *J. Med. Chem.*, **48**, 5705-5720(2005).
6) N. Moretto et al. : *Alzheimer's & Dementia*, **2**(3)Suppl 2, S110(2006).
7) B.P. Imbimbo et al. : *Alzheimer's & Dementia*, **2**(3) Suppl 2, S595(2006).
この他に以下のURLを参考にした.
γ-セクレターゼ モジュレーター　エーザイ E2012.
http://www.eisai.co.jp/news/news200618.html
8) R.C. Petersen et al. : *JAMA*, **273**, 1985-1992(1995).
9) B. Winblad et al. : *J. Intern. Med.*, **256**, 240-246 (2004).
10) T. Gomez-Isla et al. : *J. Neurosci.*, **16**, 4491-4500 (1996).
11) J.L. Price and J.C. Morris : *Ann. Neurol.*, **45**, 358-368 (1999).
12) K. Shoghi-Jadid et al. : *Am. J. Geriatr. Psychiatry*, **10**, 24-35(2002).
13) V. Kepe et al. : *Proc. Natl. Acad. Sci. USA*, **103**, 702-707(2006).
14) W.E. Klunk et al. ; *Ann. Neurol.*, **55**, 306-319(2004).
15) J.C. Price et al. : *J. Cereb. Blood. Flow. Metab.*, **25**, 1528-1547(2005).
16) B.J. Lopresti et al. : *J. Nucl. Med.*, **46**, 1959-1972 (2005).
17) H. Engler et al. : *Brain*. 2006(Jul 19)1-11(2006)doi 10.1093/brain/awl178.
18) V.L. Villemagne et al. : *Alzheimer's & Dementia*, 2(3) Suppl **2**, S325(2006).
19) NPLG. Verhoeff et al. : *Am. J. Geriatr. Psychiatry*, **12**, 584-595(2004).
20) Y. Kudo et al. : *J. Neurosci.*(submitted)(2006).
21) H. Arai et al. : *Alzheimer's & Dementia*, **2**(3)Suppl 2, S312(2006).
22) N. Okamura et al. : *J. Neurosci.*, **23**, 10857-10862 (2005).
23) W. Zhan et al. : *J. Med. Chem.*, **48**, 5980-5988(2005).
24) W. Zhan et al. : *Nucl. Med. Biol.*, **32**, 799-809(2005).
25) M. Higuchi et al. : *Nat. Neurosci.*, **8**, 527-533(2005).
26) M. Fujita et al. : Neuropsychopharmacology : The Fifth Generation of Progress, pp.411-425, Lippincott Williams & Wilkins(2002).
27) C.M. Clark et al. : *Alzheimer's & Dementia*, **2**(3)Suppl 2, S342(2006).
28) M Hintersteiner et al. : *Nat. Biotech.*, **23**, 577-583 (2003).

＜工藤　幸司／古本　祥三／岡村　信行＞

非侵襲・可視化技術ハンドブック

—ナノ・バイオ・医療から情報システムまで—

発行日 ———— 2007年 6月 25日 初版第一刷発行

監修者 ———— 小川 誠二 / 上野 照剛

発行者 ———— 吉田 隆

発行所 ———— 株式会社 エヌ・ティー・エス
〒113-0034 東京都文京区湯島 2-16-16
TEL：03(3814)9150(編集企画部)
：03(3814)9151(営業部)
http://www.nts-book.co.jp/

印 刷 ———— 株式会社 双文社印刷

製 本 ———— 牧製本印刷 株式会社

表紙デザイン ———— 岡本 秋象

ISBN978-4-86043-133-4

9 アミロイドイメージングによるアルツハイマー病の早期診断

【要約】アミロイドイメージングは、アルツハイマー病（Alzheimer's disease ; AD）の病理学的特徴である脳内Aβの沈着を生体画像化する方法である。本法を用いれば、従来の画像診断法ではできなかったADの神経病理像を評価でき、発症前段階にあるADの超早期診断も可能になると期待されている。現在、4つのPET用アミロイドイメージング剤が臨床で評価されている。画像定量解析を行うことで、健常者とAD患者を明確に判別できる結果が得られつつある。

1 はじめに

ADは、高齢者にみられる認知症の原因疾患として最も頻度の高い神経変性疾患であり、近年の急速な高齢化に伴ってその患者数は増加の一途をたどっている。さらに、ADでは臨床症状が発症してからは認知機能が進行的に低下し、予後が著しく不良であることが大きな問題となっている。現在のところADの根治療法は確立されていないが、塩酸ドネペジルやガランタミンを使うことでAD患者の認知機能や症状を一時的に改善し、病状の進行を遅らせることが可能になっている。そして、より高い効果の現れる治療を実践するためには、より早期の段階でADを確実に診断し、できる限り早く治療を開始することが重要とされている。

このような背景から、ADの早期診断法を確立することがAD研究において重要な課題の1つとなっており、核医学的手法を用いた研究も数多く行われている。そして、これまでの研究で、血流SPECTやFDG-PETによる局所脳血流・糖代謝の低下が、ADの早期診断に有効な指標となることが示されている。しかし、脳血流や糖代謝はあくまでも生理学的・生化学的変化であり、その低下は神経細胞の消失、あるいはシナプス活性の低下を反映しているとしても、その脳内局在情報を除けば必ずしもADに特異的な変化をとらえているわけではない。より感度と特異性に優れた診断法を確立するためには、疾患特異的な病理学的変化を指標とする診断方法が有効だと考えられる。

ADの場合、アミロイドβタンパク（Aβ）の脳内蓄積が疾患特異性の高い重要な病理学的変化であることから、その定量評価が可能になれば、感度および特異性に優れたAD診断法を確立することができると考えられている。このような観点から、近年非常に注目を集めているのが、Aβ蓄積の画像定量評価を目的としたアミロイドイメージングである[1,2]。この方法によるADの診断では、従来の方法と比べて診断の信頼性が大幅に向上し、原理的にADの臨床症状が現れる以前に病理状態を把握することも可能になると期待されている。本稿では、現在、世界的に激しい競争が繰り広げられているPET用アミロイドイメージング剤の開発状況について、臨床研究の成果を中心に概説する。

2 ADの病態

AD患者の脳では神経病理学的特徴として大脳皮質における老人斑（senile plaque ; SP）および神経原線維変化（neruofibrillary tangle ; NFT）の沈着、そして神経細胞の変性・脱落が観察される。

SPおよびNFTは、それぞれAβおよびリン酸化タウタンパクが異常蓄積することによって形成され、ADの病態発症機構に深く関与していると考えられている。特に、Aβの脳内蓄積はADの病態発症の最初期にみられる病理過程で、AD発症の中核をなすと考えられている（アミロイドカスケード仮説）。アミロイドカスケード仮説を

支持する研究成果の詳細は他に譲るが[3]、この仮説に基づきAD発症に至る病理変化を説明すると次のようになる。

まず、何らかの原因でAβの産生、代謝（分解）、排泄に異常をきたすことで脳内にAβの蓄積、老人斑の沈着が進行し、それによってタウタンパク質の異常蓄積、NFT形成が誘発される。そして、NFTの沈着に伴う神経細胞の変性、脱落が進行することで、最終的に臨床症状として認知機能の障害が出現することになる（図1）。

一連の病理過程は、臨床症状が発症する約10～20年前からすでに始まっていると考えられており[4]、軽度認知機能障害（mild cognitive impairment；MCI）のような臨床的には極めて早期の段階に相当する場合でも、病理学的にはすでにSP、NFT、神経細胞変性・脱落などがみられ、ADの病理像を呈することが知られている[5]。したがって、アミロイドイメージングにより脳内Aβ蓄積量を定量的に評価できるようになれば、MCIはもちろんのこと、それ以前の臨床症状が現れていない段階でもADの病理像（Aβの蓄積）を検出し、既存の検査法では不可能であったADの超早期診断が可能になると期待されている。

3　アミロイドイメージング用標識薬剤の特徴

SPを構成しているAβは、分子間でβシート構造と呼ばれる安定な二次構造をとり、線維状の凝集体を形成して存在している。アミロイドイメージングでは、その重合状態にあるAβ凝集体に特異的結合性を示す化合物の標識体をプローブとして、脳内に存在するSP（Aβ凝集体）の分布や蓄積程度を画像的に測定評価することになる。

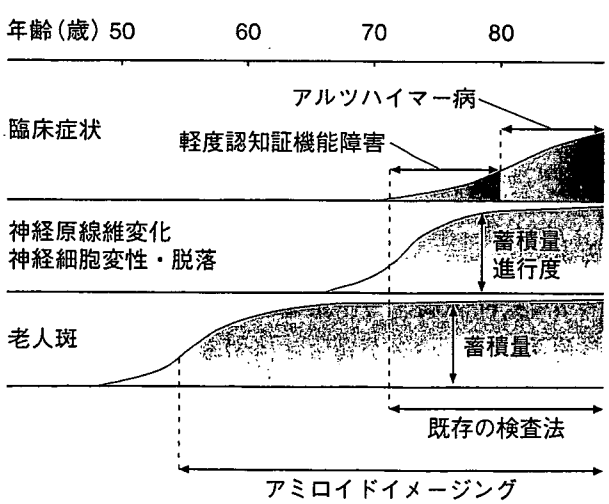

図1　アルツハイマー病における病理像と臨床像の経年変化

実際にPETでアミロイドイメージングを実現するために必要となる標識薬剤は、Aβ凝集体に対して高い結合親和性と選択性を示すと共に、投与後速やかに血液脳関門を透過して脳内へ移行し、さらに、Aβ凝集体への結合に関与しない標識薬剤は正常脳組織に非特異的結合することなく脳内から速やかに消失される、という性質を備えなくてはならない。これらの条件をほぼクリアし、臨床での評価が開始されている標識薬剤としては、以下で紹介する^{11}C-PIB、^{18}F-FDDNP、^{11}C-SB-13、^{11}C-BF227がある（図2）。

4　^{11}C-PIBの臨床評価

^{11}C-PIBは、米国ピッツバーグ大学グループによって開発されたベンゾチアゾール骨格を有するチオフラビン-T誘導体の^{11}C-メチル標識化合物であり[6～9]、現時点で最も臨床評価の進んでいる薬剤である。^{11}C-PIBの脳内集積性については、健常高齢者では、大脳皮質における放射能集積は少なく、白質領域や、脳幹に軽度の非特異的集積がみられた[8]。一方、AD患者では、SPの好発部位である大脳皮質に顕著な放射能集積を認め、健常者とは明らかに異なる集積パターンを示したが、小脳や白質領域は、健常者と同程度の集積性であった。また、FDG-PETで計測した局所糖代謝率との関連を調べてみると、^{11}C-PIBで特異的集積性を示したAD患者の大脳皮質領域では糖代謝率は減少する傾向にあり、その糖代謝率と^{11}C-PIBのSUV_{PIB}（standardized uptake value）は負の相関を示すことが確認された[8]。また、健常者—AD患者間でのSUV_{PIB}と糖代謝率について健常者対AD患者の群間差を比較した場合、SUV_{PIB}の方が統計的により有意な差がみられ、診断としてより優れていることが示唆された。

PIB-PETにおける定量解析法についてはピッツバーグ大学グループが、動脈血中放射能を入力関数とするLogan法を基準法として、種々の簡

易定量解析法の有効性を比較検討している[10,11]。結果として、小脳を参照領域とするLogan-DVR_{CER}（distribution volume ratio）やSUVR（対小脳SUV比）を指標とした場合、AD患者の後部帯状回や前頭前野の平均値は健常者と比べて約2倍程度となり、各群の個別データの分布範囲には重なりがみられず、AD患者と健常者を明確に区別することが示された[11]。Logan-DVR_{CER}やSUVRは測定再現性の精度に優れていることも確認されており、非常に有用性の高い指標であることがわかる。また、Logan-DVR_{CER}やSUVRを求める解析法では、動脈採血、代謝分析などが必要でないため、患者に対する負担の軽減や、PET検査プロトコールの大幅な簡略化が可能になるという利点もある。

ところで、同グループはMCI患者に対してもPIB-PETを実施し同様に定量解析を行っているが、その解析値は大きくばらつき、AD患者程度の値を示す症例と健常者程度の値を示す症例とが混在する結果となった（図3）[11]。この場合は、可能性としてMCI患者群にAD発症予備群に相当する進行性のAD病理像を有した患者と、ADとは異なる病態に基づく認知機能低下症患者が含まれていたと想定できる。もしそうであった場合、MCI段階においてAD発症リスクの高い患者とそうでない患者を容易に判別できている可能性がある。似たような例として、最近、Faganらは臨床症状的には異常のみられない高齢者でPIB-PETを実施し、AD患者と同様に大脳皮質領域に^{11}C-PIBの特異的集積性を示す症例を報告している[12]。彼らは、バイオマーカーとしてCSF中のタウタンパクやAβの量も同時に測定しており、その結果は完全にAD患者に分類される値を示した。この場合は無症候性のAD発症予備群に相当する症例を検出している可能性がある。このような症例については、追跡調査によって、AD発症の有無や剖検時の病理所見と^{11}C-PIB集積との関連性を調べることが重要であり、それによって初めてアミロイドイメージングコンセプトの証明、さらにはADの早期診断に対する有用性が評価されることになる。

5　^{18}F-FDDNPの臨床評価

^{18}F-FDDNPは、米国UCLAの研究グループによって開発されたアミノナフタレン骨格を有する^{18}F標識化合物であり、比較的脂溶性が高く、SPとNFTの両方に結合性を示す[13,14]。歴史的にみて、^{18}F-FDDNPは世界で最も早く臨床評価研究が開始された薬剤である。

AD患者を対象としたFDDNP-PETでは、^{18}F-FDDNP投与直後（～30分）は脳血流を強く反映するような放射能動態を示し、特に橋や後頭葉に高い放射能集積を認め、撮像の中後半以降（40分～）では、病理学的にSPやNFTの蓄積がみられる大脳皮質（側頭葉）や海馬を中心として放

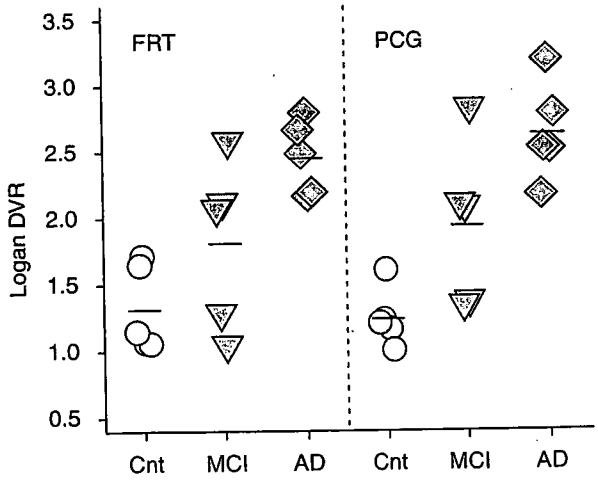

図3　^{11}C-PIBのLogan-DVR（文献10より改変）
FRT：前頭葉、PCG：後部帯状回、Cnt：健常高齢者、MCI：MCI患者、AD：AD患者

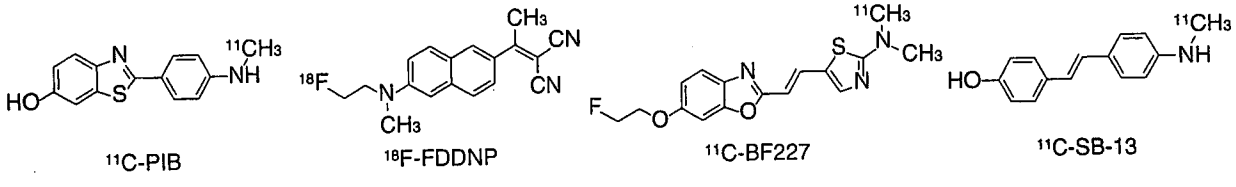

図2　現在、臨床評価が行われているPET用アミロイドイメージング剤

射能の集積がみられた[15]。FDG-PETとの比較では、^{18}F-FDDNPの集積部位である側頭葉下部で^{18}F-FDG代謝の低下がみられた。これら結果から、側頭葉領域における^{18}F-FDDNPの集積は、ある程度SPやNFTの蓄積を反映しているものと考えられる。しかし、^{18}F-FDDNPの脂溶性の高さに起因するとみられる白質や脳幹領域への非特異的集積もかなり目立ち、放射能集積画像だけから^{18}F-FDDNPの特異的集積性を目視的に評価することは難しい。

定量解析に関しては、関心領域での標識薬剤の相対的保持時間（relative retention time ; RRT）を指標とする評価手法が検討されている[15]。SPやNFTの蓄積しやすい側頭葉底部、または、海馬—扁桃体—嗅内領野でRRTを比較した場合、AD患者の場合は健常者の約2倍の値となり、両群の個別データの重なりも小さくなった。また、RRT値とMMSE（mini mental state examination）スコアの関係を調べたところ、十分に有意な負の相関を示した。しかし、RRTからは^{18}F-FDDNPの結合能（binding potential ; BP）に関する情報が得られないため、評価指標として適切かどうかについては議論の余地がある。

一方、Loganのグラフ的解析法（参照領域＝小脳）により求めたDVR（＝BP＋1）を指標として健常者とAD患者を比較した場合、内側側頭葉および後部帯状回において、AD患者のDVR平均値は健常者よりも高い値となり、MCI患者については両者のちょうど中間程度の値をとることが示された（図4）[16]。特に、MCI患者のDVR値が、PIBでみられたように大きくばらつかないという点が興味深い。これまでの神経病理学的研究では、内側側頭葉はNFTの好発部位であること、また、NFTの出現頻度は痴呆の程度によく相関することが明らかにされている。このことと合わせて考えると、内側側頭葉における^{18}F-FDDNPの集積は、NFTの集積程度を色濃く反映している可能性がある。ただし、^{18}F-FDDNPはSPとNFTの両者に結合性を示すため、基本的にはFDDNP-PETだけでどちらか一方の定量評価を行うことはできない。また、病理学的にSPとNFTの出現の仕方（量、割合など）は、脳内部位、病理の進行程度によって異なるため、たとえ定量解析値が同じ結果であっても、解析部位や病理の進行度が異なる場合には、病理像（SPとNFTの蓄積量の割合）は同じでない可能性があることに注意しなくてはいけない。

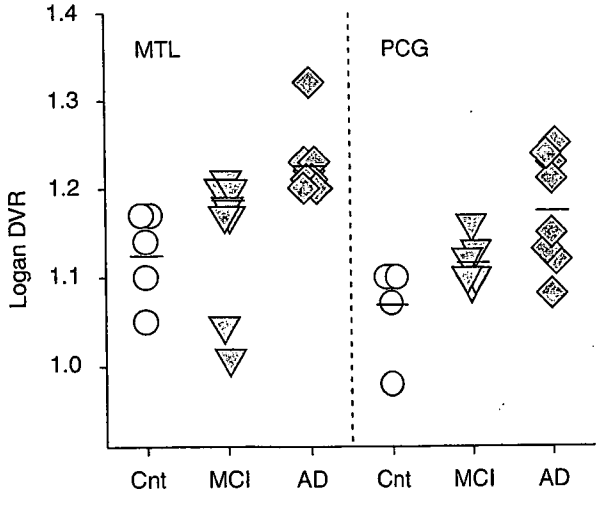

図4　^{18}F-FDDNPのLogan-DVR（文献16より改変）
MTL：内側側頭葉、PCG：後部帯状回、Cnt：健常高齢者、MCI：MCI患者、AD：AD患者

6　^{11}C-SB-13の臨床評価

^{11}C-SB-13は、米国ペンシルバニア大学グループによって開発されたスチルベン骨格を有する^{11}C-メチル標識薬剤であり[17,18]、^{11}C-PIBと比較する形で臨床評価が行われている[19]。

AD患者の脳内放射能分布については、^{11}C-SB-13と^{11}C-PIBは共に似たような分布パターンを示したが大脳皮質SUVについて健常者対AD患者の効果量（effect size）を比べたところ、^{11}C-SB-13の方が^{11}C-PIBよりも小さい値となった（平均値：1.38 vs 2.45）。すなわち、放射能集積で健常者とAD患者を比較した場合、^{11}C-SB-13では^{11}C-PIBよりも群間差が出にくいということを意味している。

定量解析で求めたBPに相当するRv値について健常者対AD患者の効果量を算出したところ、大脳皮質の平均は2.92となり、^{11}C-PIBの3.91には及ばないものの、SUVの場合よりも群間差は大きくなって、両群の個別データの重なりもほとんどみられなかった。このように、^{11}C-SB-13はRv値を指標とすることで、ADを感度よく診断

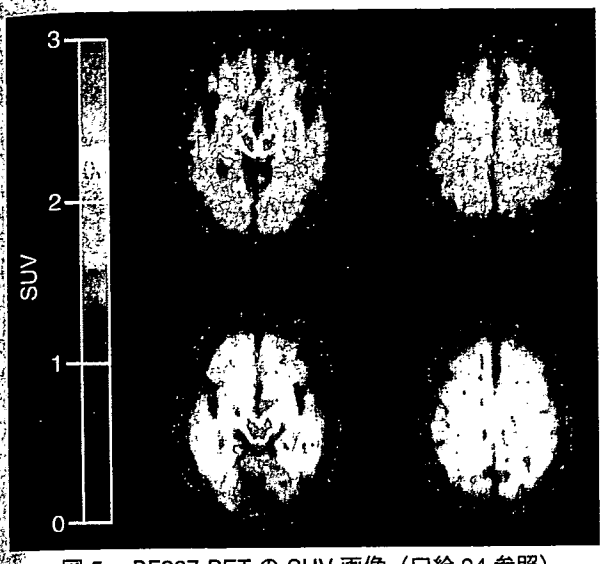

図5　BF227-PETのSUV画像（口絵94参照）
健常高齢者（上段）とAD患者（下段）における投与後30分から60分までの加算画像。

できる可能性が示唆されている。

7　^{11}C-BF227の臨床評価

^{11}C-BF227は、株式会社ビーエフ研究所および東北大学のグループによって開発された2-エテニルベンゾオキサゾール骨格を有する^{11}C-メチル標識薬剤である。2005年秋から東北大学で臨床研究が開始されている。まだ十分なデータは蓄積されていないが、これまでに明らかになった薬剤の脳内動態性についてまとめる。

健常高齢者におけるBF227-PETでは、標識薬剤投与直後には脳内全域に放射能の集積がみられ、その後は大脳皮質を中心に放射能の速やかな消失がみられた。ただし、白質領域、脳幹において軽度の非特異的集積が認められた。AD患者での検討では、投与直後は健常者と同様の集積分布を示したが、30分以降においては、老人斑の好発部位である前頭葉、側頭葉、頭頂葉などの大脳皮質領域で放射能の集積が観察され、健常者とは異なる集積像を呈した（図5）。

AD患者の大脳皮質各領域におけるSUVR（参照領域＝小脳）は、健常高齢者と比べて十分に高い値を示し、群間での個別データの重なりはほとんど認められなかった。また、^{18}F-FDDNPでみられるようなNFT好出現部位の内側側頭葉における集積はそれほど高くなかった。したがって、^{11}C-BF227は、^{11}C-PIBと同様にAD患者の大脳皮質領域においてSP特異的に集積していることが示唆され、アミロイドイメージング剤として利用可能な薬剤であると考えられる。

8　おわりに

アミロイドイメージングは、ADの早期診断にとって利用価値の高い手法であることは本稿で述べた通りだが、診断以外の利用方法に対しても高い期待が寄せられている。例えば、現在開発が進められているAD治療薬のほとんどは、脳内Aβの産生や蓄積の抑制を作用機序としているが、アミロイドイメージングは、その治療効果を評価するための有効な手段になると期待されている。また、研究的には、Aβの脳内蓄積を非侵襲的に定量評価できる利点を生かし、「アミロイドカスケード仮説」を検証するための強力なリサーチツールとして利用できると考えられている。

このように期待を持たれているアミロイドイメージングではあるが、その臨床研究はまだ途についたばかりであり、これまでの研究内容、規模ではADの早期診断に対する有効性が十分に証明されたとはいえない。ただ、これまでの研究成果だけでもアミロイドイメージングに秘められたポテンシャルの大きさを十分にうかがい知ることができる。現在、世界各国の研究機関でアミロイドイメージングの臨床研究が展開されていることから、今後、早期診断の有効性に関するエビデンスは徐々に蓄積されていくものと思われる。将来的には、研究だけでなく、一般診療や検診に広く取り入れられ、ADの早期診断や治療評価に活用されることを期待したい。

文献

1) Nordberg A: Lancet Neurol **3**: 519-527, 2004
2) Sair HI, et al: Neuroradiol **46**: 93-104, 2004
3) LaFerla FM, et al: TREND in Mol Med **11**: 170-176, 2005
4) Price JL, et al: Ann Neurol **45**: 358-368, 1999
5) Gomezisla T, et al: J Neurosci **16**: 4491-4500, 1996
6) Mathis CA, et al: J Med Chem **46**: 2740-2754, 2003
7) Klunk WE, et al: J Neurosci **25**: 10598-10606, 2005
8) Klunk WE, et al: Ann Neurol **55**: 306-319, 2004
9) Klunk WE, et al: J Neurosci **23**: 2086-2092, 2003

10) Price JC, et al: J Cereb Blood Flow Metab **25**: 1528-1547, 2005
11) Lopresti BJ, et al: J Nucl Med **46**: 1959-1972, 2005
12) Fagan AM, et al: Ann Neurol **59**: 512-519, 2006
13) Agdeppa ED, et al: J Neurosci **21**: RC189, 2001
14) Agdeppa ED, et al: Neurosci **117**: 723-730, 2003
15) Shoghi-Jadid K, et al: Am J Geriatr Psychiatry **10**: 24-35, 2002
16) Kepe V, et al: Proc Natl Acad Sci USA **103**: 702-707, 2006
17) Ono M, et al: Nucl Med Biol **30**: 565-571, 2003
18) Kung MP, et al: Brain Res **1025**: 98-105, 2004
19) Verhoeff NPLG, et al: Am J Geriatr Psychiatry **12**: 584-595, 2004

（古本祥三、岡村信行、工藤幸司）

臨床医のためのクリニカル PET
病期・病態診断のためのガイドブック

発　行　2007年6月27日　初版第1刷　©
編 集 者　クリニカル PET 編集委員会
伊藤正敏　遠藤啓吾　佐治英郎　玉木長良
畑澤　順　福田　寛　寺田弘司
発 行 者　代表取締役　寺田弘司
株式会社寺田国際事務所／先端医療技術研究所
〒112-0015　東京都文京区目白台 2-5-15-204
電話 03-5978-3141　FAX 03-6824-6570
E-mail:kterada@t3.rim.or.jp
http://www.t3.rim.or.jp/~kterada/
印　刷　株式会社ブレインズ・ネットワーク

ISBN978-4925089-18-8 C3047

定価　8,400 円（本体 8,000 円）

Printed in Japan

Imaging Amyloid Pathology in the Living Brain

Nobuyuki Okamura[a,*], Shozo Furumoto[b], Hiroyuki Arai[c], Ren Iwata[d], Kazuhiko Yanai[a] and Yukitsuka Kudo[b]

[a]Department of Pharmacology, Tohoku University School of Medicine, Sendai 980-8575, Japan, [b]Tohoku University Biomedical Engineering Research Organization (TUBERO), Sendai 980-8575, Japan, [c]Center for Asian Traditional Medicine, Department of Geriatrics and Gerontology, Tohoku University School of Medicine, Sendai 980-8574, Japan, [d]Division of Radiopharmaceutical Chemistry, Cyclotron and Radioisotope Center, Tohoku University, Sendai 980-8578, Japan

Abstract: Progressive deposition of amyloid plaques in the brain, which begins before the appearance of cognitive decline, is an initiating event in the pathogenesis of Alzheimer's disease. Therefore, noninvasive detection of amyloid pathology is important for presymptomatic diagnosis and preventive therapy for Alzheimer's disease. Recent research advances have enabled the *in vivo* imaging of amyloid pathology in humans using nuclear medicine technology. Several amyloid-binding agents have been developed and evaluated by positron emission tomography (PET) and single photon emission computed tomography (SPECT) for their use as contrast agents. Available clinical evidence indicates that amyloid imaging enables the early diagnosis of Alzheimer's disease with high accuracy and suggests its usefulness for the prediction of progression to Alzheimer's disease in subjects with mild cognitive impairment and probably also in cognitively normal individuals. Another application of this technology is as a surrogate marker for monitoring brain amyloid. In this review, we describe recent progress in the development of amyloid imaging technology and human clinical trials.

Keywords: Amyloid, Alzheimer's disease, Positron emission tomography (PET), molecular imaging, senile plaque, neurofibrillary tangle.

INTRODUCTION

Alzheimer's disease (AD) is the most common cause of dementia in the elderly. The definitive diagnosis of AD relies on postmortem assessment, with characteristic pathological changes such as neuron death, senile plaques (SPs), and neurofibrillary tangles (NFTs). Currently, the amyloid cascade hypothesis is widely accepted to account for the pathogenesis of AD [1]. SP is mainly composed of amyloid β (Aβ), which is generated by proteolytic reaction of β and γ-secretase from the amyloid precursor protein (APP). In this hypothesis, the mismetabolism of APP is the initiating event in AD pathogenesis. Excessive generation of Aβ causes aggregation of Aβ and the formation of SPs, and this is followed by the formation of NFTs, neuron death, neurotransmitter deficit, and cognitive decline. If this hypothesis is correct, optimal therapeutic strategies for interrupting the disease process should be directed toward modifying the generation, clearance, and cytotoxicity of Aβ.

Early diagnosis and treatment of AD is important in maintaining the patient's activities of daily living as long as possible and preventing the patient from becoming bedridden. A notable feature of AD is a discrepancy between clinical symptoms and pathological findings in the brain (Fig. (1)). Even in the clinically early stage of dementia, a large amount of SP is already present in the brain [2, 3]. These changes in the brain probably start 10–20 years before clinical symptoms appear. Therefore, if the deposition of SPs in the brain can be measured noninvasively, subjects who are certain to develop AD (i.e., "preclinical AD") could be screened as candidates for preventive therapy.

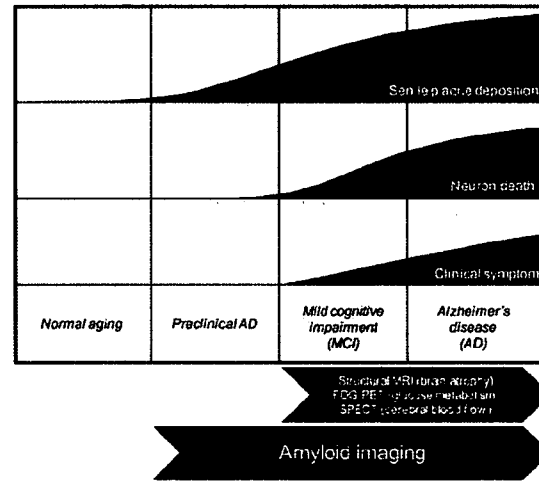

Fig. (1). Senile plaque deposition, neuron death and clinical symptom of Alzheimer's disease.

Recently, several imaging techniques, including positron emission tomography (PET), single photon emission computed tomography (SPECT), magnetic resonance imaging, and near-infrared imaging, have been developed for the noninvasive detection of SPs in AD patients. These techniques, recently classified as "amyloid imaging", are considered ideal for screening candidates for anti-amyloid therapy. PET is the most popular method for amyloid

*Address correspondence to this author at the Department of Pharmacology, Tohoku University School of Medicine, 2-1, Seiryo-machi, Aoba-ku, Sendai 980-8575, Japan; Tel: + 81-22-717-8058; Fax: +81-22-717-8060; E-mail: oka@mail.tains.tohoku.ac.jp

1573-4056/08 $55.00+.00

imaging, because of its advantages of high sensitivity, good spatial resolution, quantitative results, and ease of probe development.

DEVELOPMENT OF AMYLOID-IMAGING AGENTS

Recent advances in molecular imaging have enabled the noninvasive detection of amyloid deposits by PET or SPECT. For the high-contrast detection of amyloid deposits, imaging agents should have high binding affinity for Aβ fibrils and substantial permeability through the blood–brain barrier (BBB). Several amyloid-binding agents have been developed for the *in vivo* detection of amyloid deposits (Fig. (2)). The development of these agents started with the use of Congo red, which is commonly used for the histochemical staining of amyloid [4]. However, the BBB permeability of Congo red is limited because of its molecular size and electrostatic charge. Therefore, several Congo red derivatives have been developed with improved BBB permeability without reduced binding to amyloid [5-8]. Chrysamine-G is the first Congo red derivative that has been examined as an *in vivo* amyloid-imaging probe. However, entry of this compound into the brain is limited. Other derivatives, including BSB, ISB, and methoxy-X04, have also been developed to improve the BBB permeability. BSB successfully visualizes brain amyloid deposits in APP-transgenic mice after intravenous administration of the compound. However, this compound has insufficient BBB permeability for it to be useful as a clinical PET tracer. The first successful amyloid imaging agent to have been administered to humans is 2-(1-{6-[(2-[^{18}F]fluoroethyl)(methyl)amino]-2-naphthyl}ethylidene)malononitrile ([^{18}F]FDDNP) [9]. One of the characteristics of this agent is its ability to bind both SPs and NFTs in the AD brain. In addition, this compound is extremely lipophilic; therefore, it can penetrate the BBB more easily than previously reported compounds [10]. Interestingly, this compound binds to the same site in Aβ fibrils as non-steroidal anti-inflammatory drugs (NSAIDs) do. Therefore, this agent enables us to determine the occupancy rate of NSAIDs and experimental drugs in SPs [11]. Other candidate amyloid-imaging agents include thioflavin-T derivatives [12, 13]. N-methyl-[^{11}C]2-(4'-methylaminophenyl)-6-hydroxybenzothiazole ([^{11}C]PIB) is one such derivative and is currently the most successful amyloid-imaging agent. This compound shows high binding affinity for Aβ fibrils and SPs in AD brain homogenates, in contrast to low binding affinity for NFTs [14]. After intravenous administration, this agent shows high BBB permeability and rapid washout from normal brain tissue. Other amyloid-imaging agents, such as IMPY, stilbene, benzofuran, and acridine orange derivatives, have also been explored for use as PET and SPECT imaging probes [15-19]. The iodinated agent IMPY has been explored as a SPECT

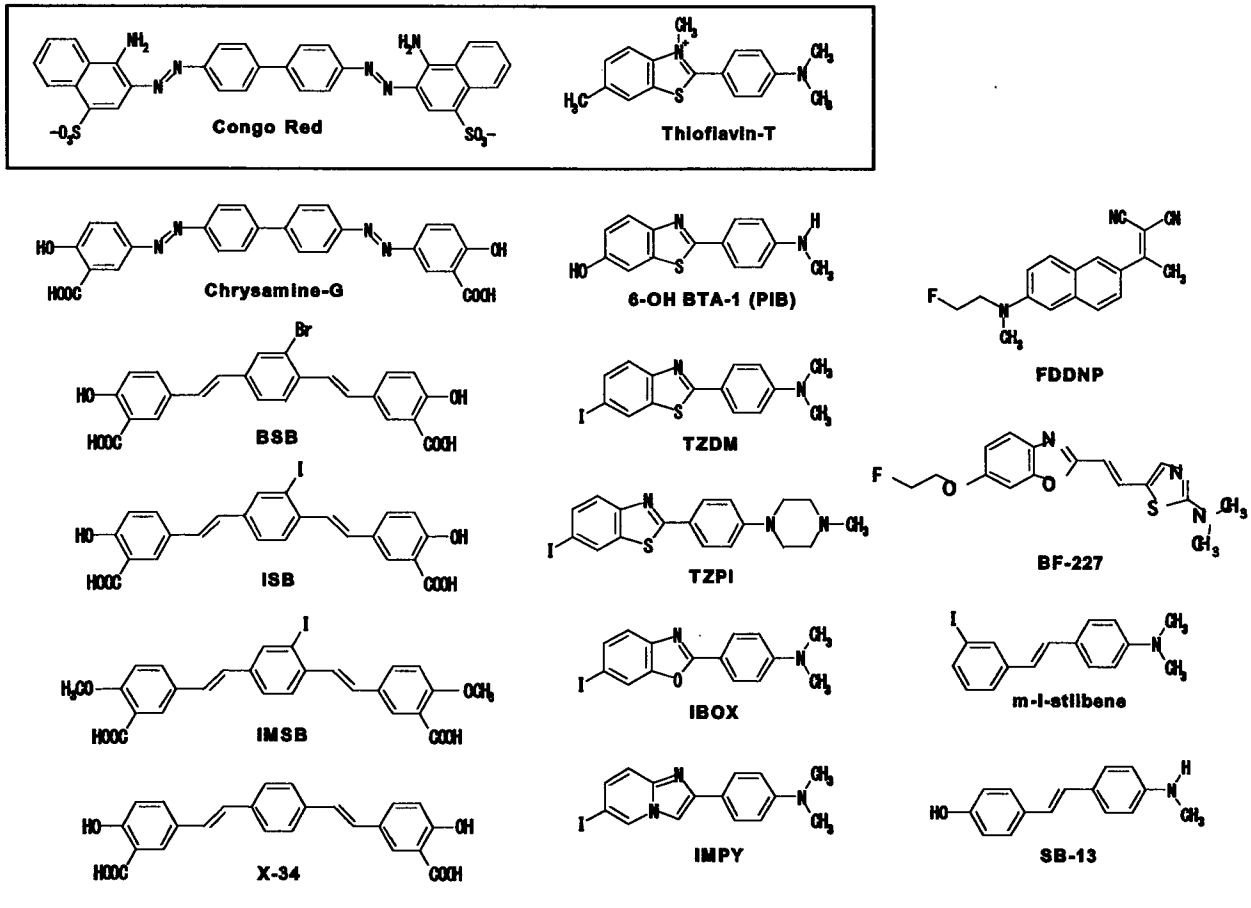

Fig. (2). Chemical structures of common imaging probes for amyloid plaques.

imaging agent and has been used in humans. Other iodinated agents are also under evaluation.

Benzoxazole derivatives are other possible amyloid-imaging agents [20-23]. Their chemical structures, binding affinities for Aβ fibrils, and pharmacokinetic data are summarized in Table 1. Most of these compounds show high binding affinity for both Aβ1-40 and Aβ1-42 fibrils. BF-191 and BF-208, which have halogens as substituents for amino groups, show low affinity for both Aβ1-40 and Aβ1-42 fibrils, suggesting that amino groups have a crucial role in binding to Aβ fibrils. All compounds have good BBB permeability. BF-227 shows faster washout from normal brain tissue than the other compounds [23, 24]. BF-227 distinctly stained SPs during the neuropathological staining of AD brain sections, and this staining pattern correlated well with Aβ immunostaining (Fig. (3)). Fluorescence microscopy revealed that this agent binds preferentially to SPs rather than NFTs. An acute and subacute toxicity study of BF-227 indicated sufficient safety for clinical use as a PET probe.

HUMAN PET STUDY

Human amyloid imaging was first studied using [^{18}F] FDDNP [9]. A [^{18}F]FDDNP PET study revealed regional accumulation of [^{18}F]FDDNP in the SP- and NFT-rich areas of the brain [25]. Global FDDNP-PET binding distinctly differentiated AD patients from normal subjects. FDDNP retention in the medial temporal lobes of subjects with mild cognitive impairment (MCI) was intermediate between levels in AD patients and normal control subjects. This finding is consistent with the observation in an autopsy study that the concentration of NFTs in the medial temporal lobes was intermediate between that in normally aging subjects and AD patients [26]. These binding characteristics indicate that this imaging agent is useful in tracing the progression of AD from the MCI stage. In addition, this agent has the potential to differentiate atypical prion disease from AD [27]. The weakness of this agent is the low signal-to-background ratio of the images, which is due to the considerable amount of nonspecific accumulation in normal brain tissue [28].

In comparison with [^{18}F]FDDNP, [^{11}C]PIB PET images differentiated AD patients from normal individuals more distinctly [29]. PIB retention was observed in the SP-rich neocortex of the brain but not in the NFT-rich medial temporal cortex, indicating that this agent binds selectively to SPs. A quantitative imaging method using PIB has already been validated [30, 31]. Over half the subjects with MCI also showed neocortical PIB accumulation to the same level as AD patients [32, 33]. Interestingly, MCI subjects who at clinical follow-up converted to AD showed higher PIB retention than subjects with non-progressive MCI, indicating that neocortical PIB retention is a marker for the prediction of progression to AD in the MCI stage [34]. A PIB-PET study in a nondemented population revealed elevated cortical retention of PIB in four nondemented persons [35]. These nondemented PIB-positive cases additionally showed an abnormality in the concentration of Aβ1-42 in cerebrospinal fluid, suggesting the presence of SPs in the absence of cognitive impairment [36]. There was a strong relationship between impaired memory performance and PIB binding in the nondemented population [37]. These findings suggest that amyloid imaging may be sensitive enough for the detection of a preclinical AD state. However, one should be careful when assessing abnormalities in the distribution of PIB, because PIB retention is also observed in cerebral amyloid angiopathy [38, 39]. Amyloid imaging may be useful as a surrogate marker for monitoring brain amyloid deposition during anti-amyloid therapy. However, longitudinal PIB-PET evaluation indicated relatively stable PIB retention after 2 years of follow-up in AD patients, suggesting that brain amyloid deposition reflected by PIB retention reaches a plateau at the early clinical stages of AD [40]. Therefore, therapy that retards the synthesis of Aβ (e.g., β- and γ-secretase inhibitors) should be started before the retention of amyloid-imaging tracers reaches a plateau.

The stilbene derivative SB-13 has also been used in a human PET study [41]. In a PET study, [^{11}C]SB-13 exhibited similar binding properties to PIB. For expanded use in clinical investigations, an ^{18}F-labeled stilbene derivative is under investigation.

A PET study using [^{11}C]BF-227 was performed at Tohoku University [23]. Neocortical retention of BF-227 was observed in an AD patient (Fig. (4)). A subject with MCI also showed cortical retention of BF-227. Interestingly, this subject was confirmed to progress to AD during the follow-up period, suggesting that cortical retention of BF-227 indicates a high risk of conversion to AD in MCI subjects. Several MCI subjects showed a distribution of BF-227 similar to that in normally aged subjects. All Alzheimer's patients and about 60% of MCI subjects showed an elevated standardized uptake value (SUV) ratio in the neocortical regions. Even in MCI subjects showing prominent retention of BF-227, the neocortical SUV ratio was below the mean value observed in AD patients. This finding suggests that MCI is a pathologically transitional state between normal aging and dementia, and that the amyloid deposition reflected by BF-227 retention does not reach a plateau in the MCI stage. Voxel-by-voxel analysis of BF-227 PET images demonstrated higher retention of BF-227 in the temporoparietal region in AD patients [23]. The pattern of distribution resembles the distribution of neuritic plaques in postmortem AD brains [42, 43]. Microscopic observation also indicates preferential binding of BF-227 to neuritic plaques in AD brain sections (Fig. (3)). In an *in vitro* binding experiment, BF-227 binding to Aβ increased linearly with increasing Aβ fibril formation [24]. For these reasons, BF-227 is considered to bind neuritic plaques selectively *in vivo*. A validation study is required to determine whether the retention of BF-227 in the neocortex accurately reflects the level of neuritic plaques rather than the level of diffuse plaques.

FUTURE DIRECTION OF PROBE DEVELOPMENT

The commercialization of ^{18}F-labeled agents or SPECT imaging agents is necessary for the wide clinical application of amyloid imaging. Because of the limited half-life of ^{11}C (20 min), the supply of ^{11}C-labeled PET agents is limited to facilities with an on-site cyclotron. ^{18}F-labeled agents are generally easier for routine clinical use because of the longer half-life of ^{18}F (110 min). Currently, several ^{18}F-labeled agents for amyloid imaging are under clinical evaluation. To

Table 1. Binding Affinity of Benzoxazole Derivatives for Aβ Fibrils and Brain Uptakes After Intravenous Administration in Normal Mice

Compounds	Chemical structure	Kd or Ki (nM)		Brain uptake (%ID/g)	
		Aβ1-40	Aβ1-42	2 min	30 min
BF-125	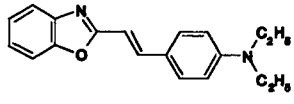	1.5 ± 0.76	4.9 ± 1.9	3.0 ± 0.87	3.0 ± 0.53
BF-133	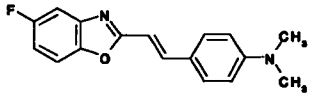	2.1 ± 1.1	3.4 ± 0.73	5.5 ± 0.40	3.8 ± 0.030
BF-140	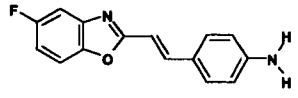	4.7 ± 2.2	2.1 ± 0.18	5.5 ± 0.60	1.1 ± 0.076
BF-145	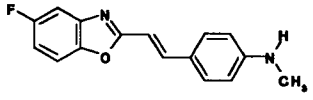	3.0 ± 0.46	4.5 ± 1.9	4.4 ± 1.80	1.6 ± 0.40
BF-168	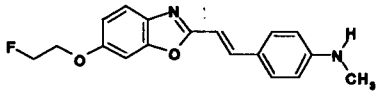	2.5 ± 2.3	6.4 ± 1.0	3.9 ± 0.22	1.6 ± 0.0071
BF-180	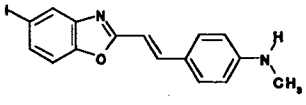	6.8 ± 1.4	10.6 ± 1.5	2.4 ± 0.52	1.8 ± 0.010
BF-185	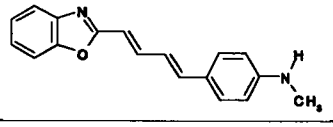	2.5 ± 2.3	14 ± 10	3.9 ± 0.49	3.8 ± 0.16
BF-191	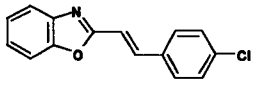	> 5000	> 5000	12 ± 0.26	1.7 ± 0.16
BF-208	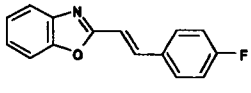	> 5000	> 5000	5.6 ± 0.64	0.28 ± 0.024
BF-227	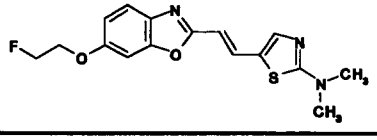	1.8 ± 0.42	4.3 ± 1.5	7.9 ± 0.18	0.54 ± 0.029

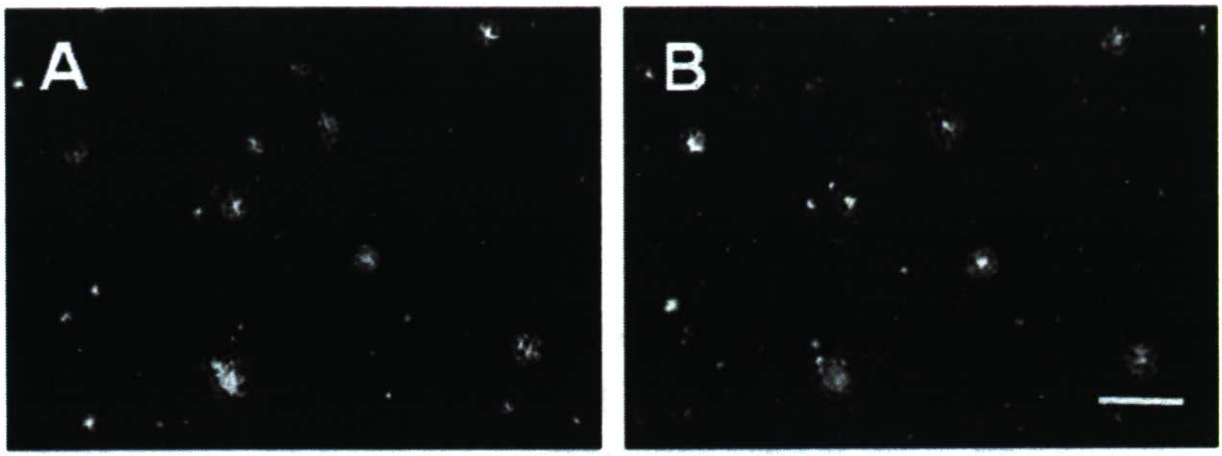

Fig. (3). Fluorescence microscopic images of senile plaques in Alzheimer's disease using BF-227 (A) and Aβ specific antibody 6F/3D (B) Bar = 100μm.

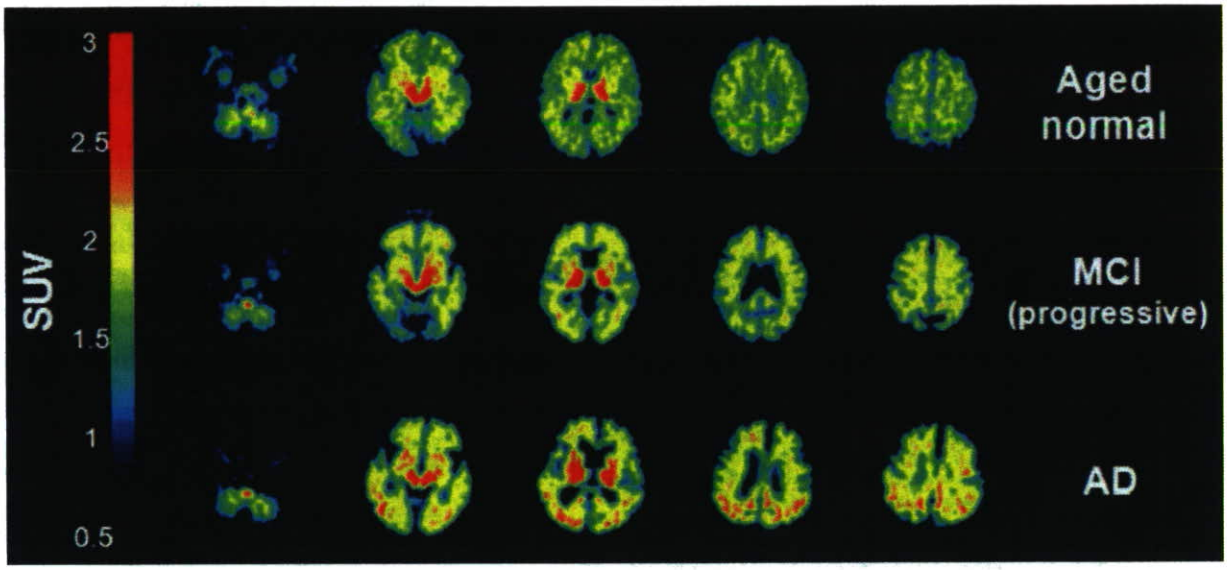

Fig. (4). Mean SUV images between 20 and 40 min post-injection of [^{11}C]BF-227 in aged normal, MCI and AD cases.

obtain a better understanding of the pathophysiology of AD, it is also necessary to visualize the distributions of Aβ pathology and tau pathology individually. However, no surrogate markers are available for evaluating the deposition of NFTs in the brain, because of the difficulty in developing a tau-specific imaging probe [44]. We previously introduced the novel compounds BF-126 and BF-170 as candidates for tau imaging [45]. In AD brain sections, BF-126 and BF-170 visualize NFTs, neuropil threads, and PHF-type neuritis distinctly. For clinical application, optimization of these compounds to reduce non-specific binding is in progress.

CONCLUSION

Several amyloid-imaging agents have been successfully developed for PET imaging. These agents displayed high binding affinity for Aβ fibrils and high BBB permeability. [^{11}C]PIB, [^{18}F]FDDNP, and [^{11}C]BF-227 displayed selective *in vivo* binding to amyloid in the brain and clearly differentiated early AD patients from normal populations. The development of ^{18}F-labeled agents or SPECT imaging agents is necessary for the wide application of amyloid imaging. The development of an NFT-specific imaging agent is also much needed. Amyloid imaging is currently the best method for the early and accurate diagnosis of AD and for monitoring amyloid pathology in the brain. This imaging technology and the forthcoming anti-amyloid therapy will cooperatively contribute to the prevention of dementia.

ACKNOWLEDGEMENTS

This study was partially supported by the Special Coordination Funds for Promoting Science and Technology, the Program for the Promotion of Fundamental Studies in Health Science of the National Institute of Biomedical Innovation, the Industrial Technology Research Grant

Program of the New Energy and Industrial Technology Development Organization (NEDO) of Japan, Health and Labour Sciences Research Grants for Translational Research from the Japanese Ministry of Health, Labour and Welfare, and a JST grant for research and education in molecular imaging.

DISCLOSURE STATEMENT

All authors have no conflict of interest.

REFERENCES

[1] Tanzi RE, Bertram L. Twenty years of the Alzheimer's disease amyloid hypothesis: a genetic perspective. Cell 2005; 120: 545-555.

[2] Goldman WP, Price JL, Storandt M, *et al.* Absence of cognitive impairment or decline in preclinical Alzheimer's disease. Neurology 2001; 56: 361-367.

[3] Price JL, Morris JC. Tangles and plaques in nondemented aging and "preclinical" Alzheimer's disease. Ann Neurol 1999; 45: 358-368.

[4] Klunk WE, Debnath ML, Pettegrew JW. Development of small molecule probes for the beta-amyloid protein of Alzheimer's disease. Neurobiol Aging 1994; 691-698.

[5] Klunk WE, Debnath ML, Pettegrew JW. Chrysamine-G binding to Alzheimer and control brain: autopsy study of a new amyloid probe. Neurobiol Aging 1995; 16: 541-548.

[6] Skovronsky DM, Zhang B, Kung MP, Kung HF, Trojanowski JQ, Lee VM. *In vivo* detection of amyloid plaques in a mouse model of Alzheimer's disease. Proc Natl Acad Sci USA 2000; 97: 7609-7614.

[7] Zhuang ZP, Kung MP, Hou C, *et al.* Radioiodinated styrylbenzenes and thioflavins as probes for amyloid aggregates. J Med Chem 2001; 44: 1905-1914.

[8] Klunk WE, Bacskai BJ, Mathis CA, *et al.* Imaging Abeta plaques in living transgenic mice with multiphoton microscopy and methoxy-X04, a systemically administered Congo red derivative. J Neuropathol Exp Neurol 2002; 61: 797-805.

[9] Shoghi-Jadid K, Small GW, Agdeppa ED, *et al.* Localization of neurofibrillary tangles and beta-amyloid plaques in the brains of living patients with Alzheimer disease. Am J Geriatr Psychiatry 2002; 10: 24-35.

[10] Agdeppa ED, Kepe V, Liu J, *et al.* Binding characteristics of radiofluorinated 6-dialkylamino-2-naphthylethylidene derivatives as positron emission tomography imaging probes for beta-amyloid plaques in Alzheimer's disease. J Neurosci 2001; 21: RC189.

[11] Agdeppa ED, Kepe V, Petri A, *et al. In vitro* detection of (S)-naproxen and ibuprofen binding to plaques in the Alzheimer's brain using the positron emission tomography molecular imaging probe 2-(1-[6-[(2-[(18)F]fluoroethyl)(methyl) amino]-2-naphthyl]ethylidene)malononitrile. Neuroscience 2003; 117: 723-730.

[12] Mathis CA, Wang Y, Klunk WE. Imaging beta-amyloid plaques and neurofibrillary tangles in the aging human brain. Curr Pharm Des 2004; 10: 1469-1492.

[13] Klunk WE, Wang Y, Huang GF, Debnath ML, Holt DP, Mathis CA. Uncharged thioflavin-T derivatives bind to amyloid-beta protein with high affinity and readily enter the brain. Life Sci 2001; 69: 1471-1484.

[14] Klunk WE, Wang Y, Huang GF, *et al.* The binding of 2-(4'-methylaminophenyl)benzothiazole to postmortem brain homogenates is dominated by the amyloid component. J Neurosci 2003; 23: 2086-2092.

[15] Kung MP, Hou C, Zhuang ZP, *et al.* IMPY: an improved thioflavin-T derivative for *in vivo* labeling of beta-amyloid plaques. Brain Res 2002; 956: 202-210.

[16] Kung HF, Kung MP, Zhuang ZP, *et al.* Iodinated tracers for imaging amyloid plaques in the brain. Mol Imaging Biol 2003; 5: 418-426.

[17] Ono M, Wilson A, Nobrega J, *et al.* ^{11}C-labeled stilbene derivatives as Abeta-aggregate-specific PET imaging agents for Alzheimer's disease. Nucl Med Biol 2003; 30: 565-571.

[18] Ono M, Kawashima H, Nonaka A, *et al.* Novel benzofuran derivatives for PET imaging of beta-amyloid plaques in Alzheimer's disease brains. J Med Chem 2006; 49: 2725-2730.

[19] Suemoto T, Okamura N, Shiomitsu T, *et al. In vivo* labeling of amyloid with BF-108. Neurosci Res 2004; 48: 65-74.

[20] Okamura N, Suemoto T, Shimadzu H, *et al.* Styrylbenzoxazole derivatives for *in vivo* imaging of amyloid plaques in the brain. J Neurosci 2004; 24: 2535-2541.

[21] Okamura N, Suemoto T, Shiomitsu T, *et al.* A novel imaging probe for *in vivo* detection of neuritic and diffuse amyloid plaques in the brain. J Mol Neurosci 2004; 24: 247-255.

[22] Furumoto S, Okamura N, Iwata R, Yanai K, Arai H, Kudo Y. Recent advances in the development of amyloid imaging agents. Curr Top Med Chem 2007; 7: 1773-1789.

[23] Kudo Y, Okamura N, Furumoto S, *et al.* 2-(2-[2-Dimethylaminothiazol-5-yl]ethenyl)-6- (2-[fluoro]ethoxy)benzoxazole: a novel PET agent for *in vivo* detection of dense amyloid plaques in Alzheimer's disease patients. J Nucl Med 2007; 48: 553-561.

[24] Okamura N, Furumoto S, Funaki Y, *et al.* Binding and safety profile of novel benzoxazole derivative for *in vivo* imaging of amyloid deposits in Alzheimer's disease. Geriatr Gerontol Int 2007 (in press)

[25] Small GW, Kepe V, Ercoli LM, *et al.* PET of brain amyloid and tau in mild cognitive impairment. N Engl J Med 2006; 355: 2652-2663.

[26] Petersen RC, Parisi JE, Dickson DW, *et al.* Neuropathologic features of amnestic mild cognitive impairment. Arch Neurol 2006; 63: 665-672.

[27] Boxer AL, Rabinovici GD, Kepe V, *et al.* Amyloid imaging in distinguishing atypical prion disease from Alzheimer disease. Neurology 2007; 69: 283-290.

[28] Bacskai BJ, Klunk WE, Mathis CA, Hyman BT. Imaging amyloid-beta deposits *in vivo*. J Cereb Blood Flow Metab 2002; 22: 1035-1041.

[29] Klunk WE, Engler H, Nordberg A, *et al.* Imaging brain amyloid in Alzheimer's disease with Pittsburgh Compound-B. Ann Neurol 2004; 55: 306-319.

[30] Price JC, Klunk WE, Lopresti BJ, *et al.* Kinetic modeling of amyloid binding in humans using PET imaging and Pittsburgh Compound-B. J Cereb Blood Flow Metab 2005; 25: 1528-1547.

[31] Lopresti BJ, Klunk WE, Mathis CA, *et al.* Simplified quantification of Pittsburgh Compound B amyloid imaging PET studies: a comparative analysis. J Nucl Med 2005; 46: 1959-1972.

[32] Rowe CC, Ng S, Ackermann U, *et al.* Imaging beta-amyloid burden in aging and dementia. Neurology. 2007; 68: 1718-1725.

[33] Kemppainen NM, Aalto S, Wilson IA, *et al.* PET amyloid ligand [^{11}C]PIB uptake is increased in mild cognitive impairment. Neurology 2007; 68: 1603-1606.

[34] Forsberg A, Engler H, Almkvist O, *et al.* PET imaging of amyloid deposition in patients with mild cognitive impairment. Neurobiol Aging 2007 (in press)

[35] Mintun MA, Larossa GN, Sheline YI, *et al.* [^{11}C]PIB in a nondemented population: potential antecedent marker of Alzheimer disease. Neurology 2006; 67: 446-452.

[36] Fagan AM, Mintun MA, Mach RH, *et al.* Inverse relation between *in vivo* amyloid imaging load and cerebrospinal fluid Abeta42 in humans. Ann Neurol 2006; 59: 512-519.

[37] Pike KE, Savage G, Villemagne VL, *et al.* Beta-amyloid imaging and memory in non-demented individuals: evidence for preclinical Alzheimer's disease. Brain 2007; 130: 2837-2844.

[38] Bacskai BJ, Frosch MP, Freeman SH, *et al.* Molecular imaging with Pittsburgh Compound B confirmed at autopsy: a case report. Arch Neurol 2007; 64: 431-434.

[39] Johnson KA, Gregas M, Becker JA, *et al.* Imaging of amyloid burden and distribution in cerebral amyloid angiopathy. Ann Neurol 2007; 62: 229-234.

[40] Engler H, Forsberg A, Almkvist O, *et al.* Two-year follow-up of amyloid deposition in patients with Alzheimer's disease. Brain 2006; 129: 2856-2866.

[41] Verhoeff NP, Wilson AA, Takeshita S, *et al.* In-vivo imaging of Alzheimer disease beta-amyloid with [^{11}C]SB-13 PET. Am J Geriatr Psychiatry 2004; 12: 584-595.

[42] Arnold SE, Hyman BT, Flory J, Damasio AR, Van Hoesen GW. The topographical and neuroanatomical distribution of neurofibrillary tangles and neuritic plaques in the cerebral cortex of patients with Alzheimer's disease. Cereb Cortex 1991; 1: 103-116.

[43] Cummings JL, Cole G. Alzheimer disease. JAMA 2002; 287: 2335-2338.

[44] Small GW, Agdeppa ED, Kepe V, Satyamurthy N, Huang SC, Barrio JR. *In vivo* brain imaging of tangle burden in humans. J Mol Neurosci 2002; 19: 323-327.

[45] Okamura N, Suemoto T, Furumoto S, *et al.* Quinoline and benzimidazole derivatives: candidate probes for *in vivo* imaging of tau pathology in Alzheimer's disease. J Neurosci 2005; 25: 10857-10862.

Received: December 5, 2007 Revised: December 7, 2007 Accepted: December 10, 2007

2-(2-[2-Dimethylaminothiazol-5-yl]Ethenyl)-6-(2-[Fluoro]Ethoxy)Benzoxazole: A Novel PET Agent for In Vivo Detection of Dense Amyloid Plaques in Alzheimer's Disease Patients

Yukitsuka Kudo[1], Nobuyuki Okamura[2], Shozo Furumoto[1], Manabu Tashiro[3], Katsutoshi Furukawa[4], Masahiro Maruyama[4], Masatoshi Itoh[3], Ren Iwata[5], Kazuhiko Yanai[2], and Hiroyuki Arai[4]

[1]Tohoku University Biomedical Engineering Research Organization (TUBERO), Sendai, Japan; [2]Department of Pharmacology, Tohoku University School of Medicine, Sendai, Japan; [3]Division of Cyclotron Nuclear Medicine, Cyclotron and Radioisotope Center, Tohoku University, Sendai, Japan; [4]Department of Geriatrics and Gerontology, Center for Asian Traditional Medicine, Tohoku University School of Medicine, Sendai, Japan; and [5]Division of Radiopharmaceutical Chemistry, Cyclotron and Radioisotope Center, Tohoku University, Sendai, Japan

Extensive deposition of dense amyloid fibrils is a characteristic neuropathologic hallmark in Alzheimer's disease (AD). Noninvasive detection of these molecules is potentially useful for early and precise detection of patients with AD. This study reports a novel compound, 2-(2-[2-dimethylaminothiazol-5-yl]ethenyl)-6-(2-[fluoro]ethoxy)benzoxazole (BF-227), for in vivo detection of dense amyloid deposits using PET. **Methods:** The binding affinity of BF-227 to amyloid-β (Aβ) fibrils was calculated. The binding property of BF-227 to amyloid plaques was evaluated by neuropathologic staining of AD brain sections. Brain uptake and in vivo binding of BF-227 to Aβ deposits were also evaluated using mice. For clinical evaluation of ^{11}C-BF-227 as a PET probe, 11 normal (healthy) subjects and 10 patients with AD participated in this study. Dynamic PET images were obtained for 60 min after administration of ^{11}C-BF-227. The regional standardized uptake value (SUV) and the ratio of regional to cerebellar SUV were calculated as an index of ^{11}C-BF-227 retention. The regional tracer distribution in AD patients was statistically compared with that of aged normal subjects on a voxel-by-voxel basis. **Results:** BF-227 displayed high binding affinity to synthetic Aβ1-42 fibrils (K_i [inhibition constant], 4.3 ± 1.5 nM). Neuropathologic staining has demonstrated preferential binding of this agent to dense amyloid deposits in AD brain. Moreover, a biodistribution study of this agent revealed excellent brain uptake and specific labeling of amyloid deposits in transgenic mice. The present clinical PET study using ^{11}C-BF-227 demonstrated the retention of this tracer in cerebral cortices of AD patients but not in those of normal subjects. All AD patients were clearly distinguishable from normal individuals using the temporal SUV ratio. Voxel-by-voxel analysis of PET images revealed that cortical BF-227 retention in AD patients is distributed primarily to the posterior association area of the brain and corresponded well with the preferred site for neuritic plaque depositions containing dense Aβ fibrils. **Conclusion:** These findings suggest that BF-227 is a promising PET probe for in vivo detection of dense amyloid deposits in AD patients.

J Nucl Med 2007; 48:553–561
DOI: 10.2967/jnumed.106.037556

Substantial neuropathologic evidence suggests that the deposition of senile plaques (SPs) and neurofibrillary tangles (NFTs) represents the characteristic neuropathologic hallmark in Alzheimer's disease (AD) (*1*). Progressive accumulation of SPs is considered fundamental to the initial development of dementia. Extensive deposition of SPs in the brain is present even in very mild AD and precedes the presentation of cognitive impairment (*2,3*). Several antiamyloid drugs are under development for the treatment and prevention of AD (*4*). For early detection and preventive intervention for AD, noninvasive imaging of neuropathologic lesions is a powerful strategy.

For this purpose, several imaging techniques have been developed that can noninvasively detect SPs in the brain using PET, SPECT, and MRI. Among these imaging modalities, PET is the most advanced and practical method for in vivo measurement of SP depositions. To achieve successful imaging using PET, various radiolabeled agents have been developed. Currently, 6OH-BTA-1 (PIB) is the most successful PET agent for in vivo amyloid imaging. This tracer sensitively detects amyloid fibrils in the brain and is proven to be useful for early diagnosis of AD (*5–7*).

However, amyloid-β (Aβ) deposition is also frequent in aging, even in cognitively intact individuals. Excessive identification of Aβ has a potential risk to misjudge the normal aging process with abnormal Aβ deposition. In the

Received Oct. 23, 2006; revision accepted Jan. 20, 2007.
For correspondence or reprints contact: Nobuyuki Okamura, MD, Department of Pharmacology, Tohoku University School of Medicine, 2-1, Seiryo-machi, Aoba-ku, Sendai 980-8575, Japan.
E-mail: oka@mail.tains.tohoku.ac.jp

normal aging process, noncompact or diffuse amyloid plaques containing less fibrillar Aβ are deposited primarily in the brain. Brains from patients with AD are characterized by an anatomically widespread process of amyloid deposition and neuritic plaque formation containing dense amyloid fibrils (*8*). A shift of brain Aβ from the soluble to the fibrillar form is closely associated with the onset of AD (*9*). Therefore, selective detection of dense amyloid fibrils would be advantageous to differentiate the normal aging process from AD with high specificity.

We have previously demonstrated a novel series of benzoxazole derivatives as promising candidates for an in vivo imaging probe of SPs (*10–12*). These derivatives showed comparatively high blood–brain barrier (BBB) permeability, high binding affinity for Aβ aggregates, and high specificity for fibrillar Aβ deposits, suggesting potential merit for the early detection of AD-related pathologies. Herein we introduce an optimized derivative, 2-(2-[2-dimethylaminothiazol-5-yl]ethenyl)-6-(2-[fluoro]ethoxy)benzoxazole (BF-227), as a PET probe for in vivo detection of dense amyloid deposits in humans.

MATERIALS AND METHODS

Preparation of Compounds

BF-227 (Fig. 1) and its *N*-desmethylated derivative (a precursor of ^{11}C-BF-227) were custom-synthesized by Tanabe R&D Service Co. ^{11}C-BF-227 was synthesized from the precursor by *N*-methylation in dimethyl sulfoxide (Fig. 1) using ^{11}C-methyl triflate (*13,14*). After quenching the reaction with 5% acetic acid in ethanol, ^{11}C-BF-227 was separated from the crude mixture by semipreparative reversed-phase high-performance liquid chromatography and then isolated from the collected fraction by solid-phase extraction. The purified ^{11}C-BF-227 was solubilized in isotonic saline containing 1% polysobate-80 and 5% ascorbic acid. The saline solution was filter-sterilized with a 0.22-μm Millipore filter for clinical use. The radiochemical yields were >50% based on ^{11}C-methyl triflate, and the specific radioactivities were 119–138 GBq/μmol at the end of synthesis. The radiochemical purities were >95%.

In Vitro Binding Assays

Binding affinities of the compounds for synthetic Aβ1-42 aggregates were examined as described previously (*10*). Briefly, solid-form Aβ1-42 (Peptide Institute) was dissolved in 10 mM potassium phosphate buffer (pH 7.4) and incubated at 37°C for 40 h. The binding assay was performed by mixing 100 μL of aggregated Aβ1-42 with the appropriate concentration of ^{125}I-labeled 2-(4-methylamino)styryl-5-iodo-benzoxazole (BF-180) and 8% ethanol. After incubation for 4 h at room temperature, the binding mixture was filtered and filters containing bound ^{125}I ligand were counted using a γ-counter. The dissociation constant (K_d) and maximum specific binding (B_{max}) of BF-180 were determined. For inhibition studies, binding studies were performed using synthetic Aβ1-42 aggregates. A mixture containing 50 μL of BF-227, 50 μL of 0.05 nM ^{125}I-BF-180, 100 μL of 100 nM Aβ1–42, and 800 μL of 8% ethanol was incubated at room temperature for 4 h. The mixture was then filtered through Whatman GF/B filters, and filters containing bound ^{125}I ligand were counted in a γ-counter. Values for the half-maximal inhibitory concentration (IC_{50}) were determined from displacement curves of 3 independent experiments using Prism software (GraphPad), and values for the inhibition constant (K_i) were determined using the Cheng–Prusoff equation.

Measurement of Octanol/Water Partition Coefficients

Phosphate-buffered saline (PBS) and 1-octanol (Wako) were saturated with 1-octanol and PBS, respectively, before use. BF-227 was dissolved in 1-octanol and shaken with equal amounts of PBS for 30 min at room temperature. After centrifugation at 2,000 rpm for 15 min, absorbency of the 1-octanol layer was measured at the peak wavelength of the absorbance spectrum of BF-227 using a Spectra Max 190 microplate reader (Molecular Devices). Octanol/water partition coefficients were determined by comparing absorbency with that before shaking with PBS. Each data point was performed in duplicate.

BBB Permeability of BF-227 in Normal Mice

Brain uptake of BF-227 was measured using ^{11}C-labeled compound. The ^{11}C-BF-227 (1.1–6.3 MBq) was administered into the tail vein of male C57B6 mice (n = 23; mean weight, 28–32 g). Mice were then sacrificed by decapitation at 2, 10, 30, and 60 min after injection. The whole brain was removed and weighed, and radioactivity was counted using an automatic γ-counter. The percentage injected dose per gram of tissue (%ID/g) was calculated by normalizing tissue counts to tissue weight. Each %ID/g value is expressed as a mean ± SD of 3 or 4 separate experiments.

Neuropathologic Staining

Postmortem brain tissues from a 69-y-old man with autopsy-confirmed AD and an 81-y-old man with autopsy-confirmed physiologic aging were obtained from Fukushimura Hospital (Toyohashi, Japan). Experiments were performed under the regulations of the ethics committee of BF Research Institute. Serial sections (6-μm thick) from paraffin-embedded blocks of temporal cortex, striatum, and cerebellum were prepared in xylene and ethanol. Before

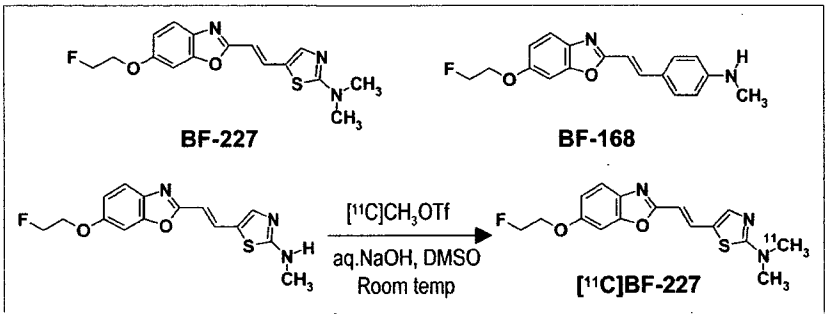

FIGURE 1. Chemical structures of BF-227 and BF-168 and radiosynthesis of BF-227.

the staining of compounds, quenching of autofluorescence was performed as described previously. Quenched tissue sections were immersed in 100 μM of BF-227 or 0.125% thioflavin-S solution containing 50% ethanol for 10 min. Sections stained with each compound were then dipped briefly into water and rinsed in PBS for 60 min before coverslipping with Fluor Save Reagent (Calbiochem); sections were examined using an Eclipse E800 microscope (Nikon) equipped with a V-2A filter set (excitation, 380–420 nm; dichroic mirror, 430 nm; long-pass filter, 450 nm). Sections stained with thioflavin-S were dipped briefly in tap water and in 50% ethanol and then washed in PBS for 60 min before coverslipping; this was followed by fluorescent microscopy using a BV-2A filter set (excitation, 400–440 nm; dichroic mirror, 455 nm; long-pass filter, 470 nm). In addition, adjacent sections were immunostained using monoclonal antibody (mAb) against Aβ (6F/3D; Dako A/S). After pretreatment with 90% formic acid for 5 min, sections were immersed in blocking solution for 30 min and then incubated for 60 min at 37°C with 6F/3D at a dilution of 1:50. After incubation, sections were processed by the avidin–biotin method using a Pathostain ABC-POD(M) Kit (Wako) and diaminobenzidine tetrahydrochloride.

Labeling of Aβ Deposits in Transgenic Mouse Brain

Ex vivo plaque labeling with BF-227 was evaluated using PS1/APPsw double transgenic mice (n = 2) and a wild-type mouse (n = 1) (male, 32-wk old) (*15*). A BF-227 solution containing 10% polyethylenglycol 400 and 0.1 mol/L HCl was administered into the tail vein at a dose of 4 mg/kg. Mice were anesthetized using sodium pentobarbital 2 h after injection of BF-227; they were then perfused transcardially with ice-cold saline, which was followed by 4% paraformaldehyde in 0.1 M PBS, and the brains were removed. After cryoprotection in 30% sucrose/0.1 M PBS, 6-μm frozen sections were cut using an OTF cryostat and imaged with no additional staining for fluorescent microscopy using a V-2A filter set. The same sections were immunostained using mAb against Aβ (6F/3D) as described earlier.

Subjects and Patients in Clinical PET Study

Eleven normal (healthy) control subjects, including 3 young normal subjects and 8 aged-matched normal subjects, and 10 probable AD patients underwent PET measurement of ^{11}C-BF-227 distribution in the brain (Table 1). AD patients were recruited through the Tohoku University Hospital Dementia Patients Registry. The diagnosis of AD was made according to the National Institute of Neurological and Communicative Diseases and Stroke/Alzheimer's Disease and Related Disorders Association (NINCDS–ADRDA) criteria. The normal control group was recruited from volunteers, who were taking no centrally acting medication, had no cognitive impairment, and had no cerebrovascular lesion on MR images. No significant difference in age was apparent between the AD group and the aged normal control group. AD patients had significantly lower mean mini-mental status examination (MMSE) scores than normal control subjects. This study was approved by the ethics committee on clinical investigations of Tohoku University School of Medicine and was performed in accordance with the Declaration of Helsinki. After complete description of the study to the patients and subjects, written informed consent was obtained.

Image Acquisition Protocols

The protocol of the PET study was approved by the Committee on Clinical Investigation at The Tohoku University School of Medicine and the Advisory Committee on Radioactive Substances at Tohoku University. The ^{11}C-BF-227 PET study was performed using a SET-2400W PET scanner (Shimadzu). After intravenous injection of 211–366 MBq of ^{11}C-BF-227, dynamic PET images were obtained for 60 min (23 sequential scans: 5 scans × 30 s, 5 scans × 60 s, 5 scans × 150 s, and 8 scans × 300 s) with each subject's eyes closed. The T1-weighted MR images were obtained using a SIGNA 1.5-T machine (GE Healthcare).

TABLE 1
Subject Demographics

Group	Subject	Sex	Age (y)	MMSE score
Young normal (n = 3)	YN 1	M	36	30
	YN 2	M	37	30
	YN 3	M	36	30
	Mean ± SD		36.3 ± 0.6	30.0 ± 0.0
Aged normal (n = 8)	AN 1	M	69	30
	AN 2	F	70	29
	AN 3	F	64	30
	AN 4	F	65	30
	AN 5	M	67	30
	AN 6	M	69	30
	AN 7	M	71	30
	AN 8	M	59	30
	Mean ± SD		66.8 ± 4.0	29.9 ± 0.4
All normal (n = 11)	Mean ± SD		58.5 ± 14.6	29.9 ± 0.3
AD (n = 10)	AD 1	F	65	24
	AD 2	M	75	19
	AD 3	F	72	21
	AD 4	F	82	18
	AD 5	F	62	20
	AD 6	F	68	21
	AD 7	M	70	23
	AD 8	F	85	23
	AD 9	M	78	14
	AD 10	F	75	26
	Mean ± SD		73.2 ± 7.3*	20.9 ± 3.4*†

*P < 0.05 vs. young normal group.
†P < 0.05 vs. aged normal group.
MMSE = mini-mental state examination.

Image Analysis

First, standardized uptake value (SUV) images of ^{11}C-BF-227 were obtained by normalizing tissue radioactivity concentration by injected dose and body weight. Subsequently, individual MR images were anatomically coregistered into individual PET images using Statistical Parametric Mapping software (SPM2; Wellcome Department, U.K.) (*16*). Regions of interest (ROIs) were placed on individual axial MR images in the cerebellar hemisphere, striatum, thalamus, frontal cortex (Brodmann's areas [BA] 8, 9, 10, 44, 45, 46, and 47), lateral temporal cortex (BA 21, 22, 37, and 38), parietal cortex (BA 39 and 40), temporooccipital cortex (BA 18 and 19), occipital cortex (BA 17), medial temporal cortex (BA 27, 28, 34, and 35), pons, and subcortical white matter, as described previously (*17*). The ROI information was then copied onto dynamic PET SUV images, and regional SUVs were sampled using Dr.View/LINUX software (Asahi-Kasei Joho System).

The interrater reliability for the ROI measurement was tested between 2 raters in 14 subjects and patients. The intraclass correlation coefficient was 0.95 in the frontal cortex and cerebellum, 0.97 in the lateral temporal and parietal cortices, and 0.98 in the medial temporal cortex. The correlation coefficient between these 2 measurements was 0.96 in the frontal cortex, 0.97 in the lateral temporal cortex, and 0.99 in the parietal cortex, medial temporal cortex, and cerebellum. SUVs between 40 and 60 min were averaged to calculate the SUVs for group comparison.

Statistical Analysis

For statistical comparison in the 3 groups, we applied the Kruskal–Wallis test, which was followed by Dunn's multiple comparison test. The difference in time–activity curves in ^{11}C-BF-227 PET was also evaluated by repeated measures ANOVA, which was followed by the Bonferroni–Dunn post hoc test. For statistical comparisons of PET measurements in aged normal and AD groups, we used the Mann–Whitney *U* test. Effect-size coefficients (Cohen's *d*) were also calculated for the evaluation of group differences in PET measurements. Statistical significance for each analysis was defined as $P < 0.05$. Statistical comparison between images from normal control subjects and AD patients was performed on a voxel-by-voxel basis using SPM2 software (*16*). SUV summation images 30–60 min after injection were stereotactically normalized using individual MR images into a standard space of Talairach and Tournoux. The normalized images were smoothed using a $16 \times 16 \times 16$ mm gaussian filter. The count of each voxel was normalized to the cerebellar ROI value, because cerebellum is reported to be a region free of fibrillar amyloid plaques in AD brain. Images of patients with AD ($n = 10$) were compared with those of aged normal control subjects ($n = 8$) for between-group analysis ($P < 0.001$, uncorrected; extent threshold, $k = 200$). For the group analysis, a 2-sample *t* test was used to detect differences between the AD and normal control groups.

RESULTS

In Vitro Binding Study for Aβ Fibrils

In vitro binding assay indicated that BF-227 shows high binding affinity for Aβ1-42 fibrils. K_i for Aβ1-42 fibrils in competitive binding assay using ^{125}I-BF-180 was 4.3 ± 1.5 nM in BF-227, comparable to levels previously reported for compound BF-168.

Neuropathologic Staining in AD Brain Sections

Neuropathologic examination using BF-227 indicated that amyloid plaques were selectively stained with BF-227 in AD brain sections (Fig. 2A). Especially, cored plaques were brightly stained with BF-227, indicating that this compound preferentially binds to mature amyloid plaque. This staining pattern correlated well with Aβ immunostaining in adjacent sections (Fig. 2B, arrows). BF-227 staining was further compared with staining using thioflavin-S. In contrast to clear staining of SPs and NFTs with thioflavin-S (Fig. 2C), BF-227 primarily stained SPs, with faint staining of NFTs (Fig. 2B, arrowheads). No apparent staining was also observed in the temporal brain section of the aged normal case (Fig. 2D).

BBB Permeability and Clearance from Normal Brain

Next, we investigated whether BF-227 entered the brain in amounts sufficient for use as a PET agent. The log *P* value of BF-227 was 1.75, close to that of BF-168 (log $P = 1.79$). Intravenous administration of BF-227 into normal mice indicated that this compound readily penetrated the BBB. Brain uptakes at 2, 10, 30, and 60 min after intravenous injection of ^{11}C-BF-227 were 7.9 ± 1.3, 3.7 ± 0.37, 1.4 ± 0.36, and 0.64 ± 0.15 %ID/g, respectively. ^{11}C-BF-227 displayed double the initial uptake and faster washout

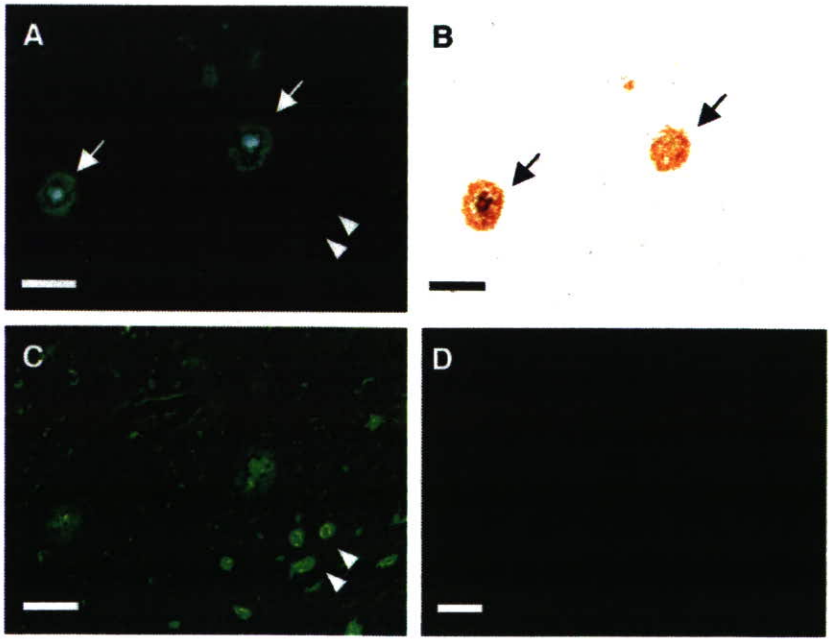

FIGURE 2. Neuropathologic staining of human brain sections by BF-227. Amyloid plaques are clearly stained with BF-227 in AD temporal brain sections (A). BF-227 staining correlates well with Aβ immunostaining in adjacent sections (B, arrows). BF-227 faintly stains NFTs, in contrast to clear staining with thioflavin-S (C, arrowheads). In aged normal temporal cortex (D), no staining by BF-227 is observed. Bar in A–C = 50 μm; bar in D = 200 μm.